Analysis of Fast-Scanning Data from ALMA*

Benjamin Gill†

Project Supervisor: Prof Richard Hills

May 14, 2015

Abstract

Fast-scanning uses a single 12 m antenna at the Atacama Large Millimeter/submillimeter Array (ALMA) to physically scan a region of interest. This can be used to probe angular resolutions greater than those achievable with ALMA in its interferometric operation. The data is converted to brightness temperature, and then the noise present is analysed. There is a substantial atmospheric component to the noise, which can be partially removed as part of the map-making process. Three means of undertaking the removal are investigated and basket weaving is found to be superior, removing 60% of the noise whilst being computationally inexpensive.

1 Introduction

Inaugurated in 2013, the Atacama Large Millimeter/submillimeter Array (ALMA) is an international radio telescope in the Atacama Desert in Chile.[1] It consists of an array of 66 antennae, observing at wavelengths of 0.3–10 mm.[2] This work deals solely with the 12 m diameter antennae, of which there are 54.

In normal operation, these are used in an interferometric array, with baselines of up to 15 km giving a finest angular resolution of 0.015" at a wavelength

*Source code available at `http://bjg43.user.srcf.net/`. Additional data available at `http://www.mrao.cam.ac.uk/~richard/ALMA_Scan/`

†Queens' College, Cambridge, bjg43@cam.ac.uk

of 1 mm.[4] However, interferometry imposes a maximum angular scale (due to the Fourier transform of the finite spacing between the dishes making up the array), which is of the order of 20" at a wavelength of 1 mm.

Thus, to produce images of large-scale objects, many interferometric observations of small patches of sky must be built up into a 'mosaic' image. An alternative approach is required to obtain the large-scale structure. In this paper, the fast-scanning method is used.

Fast-scanning consists of rapidly scanning a single telescope over the region of interest. The true pointing of the telescope can be measured to a sufficient accuracy that the angular resolution is limited by the beam width of the telescope – 17" at a wavelength of 1 mm.[4] The area of sky able to be observed is limited by the need to observe near the zenith to minimise atmospheric noise and the need for sufficient coverage of that area. Fast-scanning has been tested for areas of up to 140 square arcminutes.

However, since a single dish is being used, atmospheric and electronic noise become significant. Reduction of the electronic noise requires long observing times. By contrast, atmospheric noise, being low frequency, is amenable to reduction through the use of appropriate algorithms, as described in this work.

The rest of the report is organised as follows. The observational techniques are described in section 2. Section 3 gives an explanation of the method used to convert intensity to temperature data. The characterisation of the noise present is described in section 4. Then, the methods used to produce maps and remove noise are explained and evaluated in section 5, before conclusions are offered in section 6.

2 Observational Technique

The antenna gathers signal separately in two orthogonal polarisations (X and Y). The signal is then filtered into four bands of 2 GHz, down sampled, amplified and digitised. This produces a total of eight channels of data, which should have partially uncorrelated noise. A typical observation lasts 400–500 s.

The optimal observing strategy would be a random sampling across the region of interest.[10] With a real telescope, one is mechanically limited, so a scanning pattern is required. A good coverage can be obtained using a Lissajous

pattern (figure 1). For a circular area, a 'clover-leaf' central scanning pattern has the advantage of concentrating observational weight at the centre of the map, which is useful for compact sources.

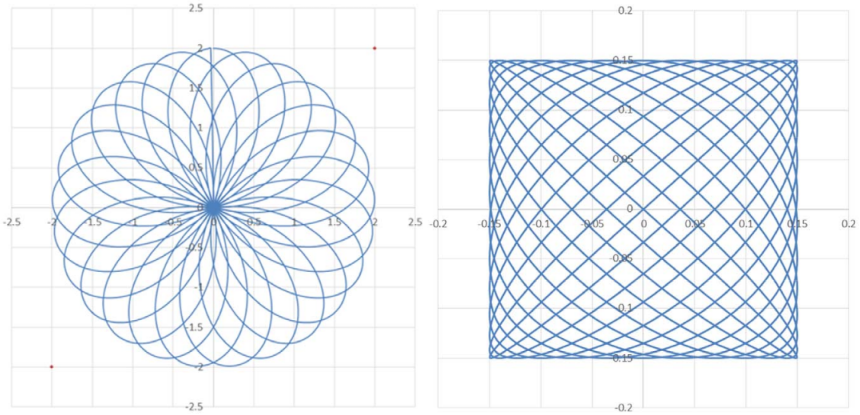

Figure 1: Two possible patterns for scanning: central and Lissajous

The raw data come in two files: one contains the pointing data, sampled at 21 Hz, and the other the signal, sampled at 500 Hz. A pointing must be assigned to each signal reading. Thus, the first step is to interpolate the pointing data to assign a pointing to each signal reading. This is done using a cubic spline.

3 Data Conversion

Equation 1 gives the model used for the signal, S, received from a source of brightness temperature T_{obs}. G is a constant gain and O a constant offset. T_{obs}, T_{CMB}, T_{atm} and T_{sys} are the CMB (2.73 K), atmospheric and systematic temperatures, respectively.

$$S = (T_{\text{obs}} + T_{\text{CMB}} + T_{\text{atm}} + T_{\text{sys}})\, G + O \tag{1}$$

As seen in figure 2, six sets of data are taken. Calibration is performed by observing a patch of 'blank' sky near the source of interest, yielding $S_{\text{blank}} = (T_{\text{CMB}} + T_{\text{atm}} + T_{\text{sys}})\, G + O$. Then, two reference loads are put in front of the antenna ($S_{\text{ref}} = (T_{\text{sys}})\, G + O$), to give the full set of constants to convert the data to a temperature scale.

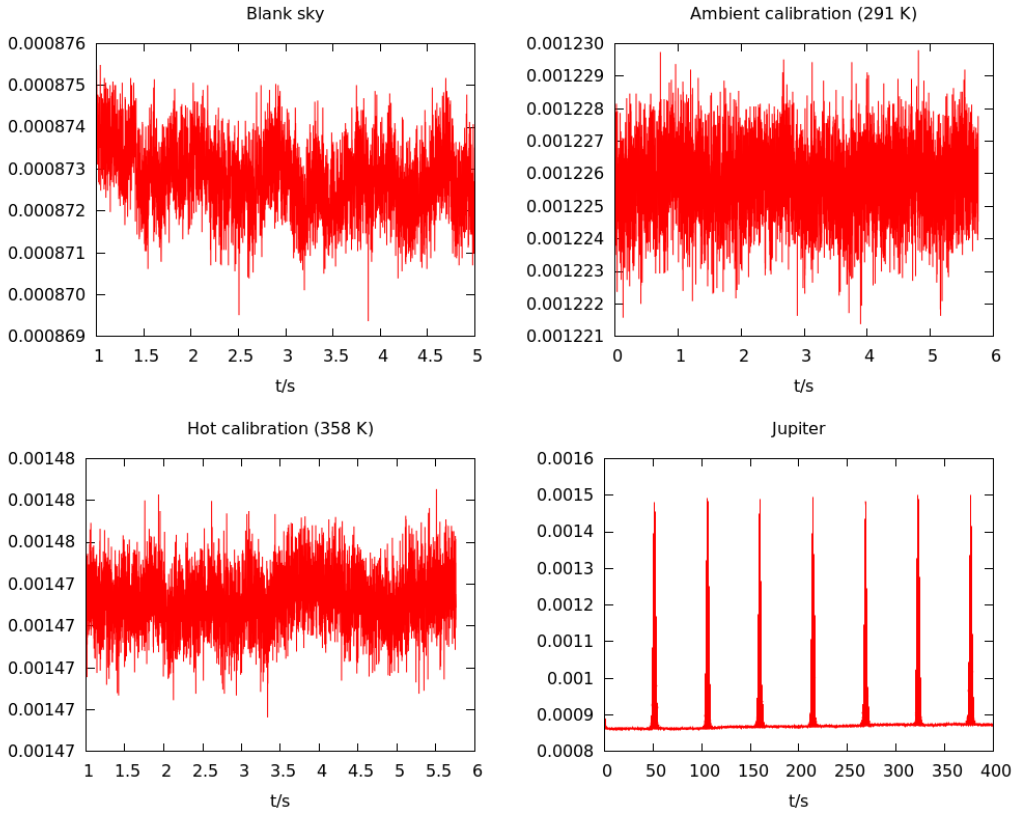

Figure 2: Calibration

3.1 Discussion

The results of this conversion are shown in figure 3, which is the conversion of the data given in figure 2. In this case, Jupiter was being observed. The peak value for each pass is about 165K, which is consistent with previous measurements of the brightness temperature of Jupiter.[8] The drift in the 'zero' measurement is clear evidence of atmospheric noise.

However, the simple model for the observed signal (equation 1) does not take into account the optical depth of the atmosphere, which has been previously measured to have a zenith median value of 0.061 at 230 GHz.[1] This will have the effect of underestimating the true sky temperature. However, the optical depth is highly variable, having 25% and 75% points in the distribution of 0.036 and 0.115. Ideally, one would want to measure the optical depth at the time of the observation, or produce a modelled value based on atmospheric observables.

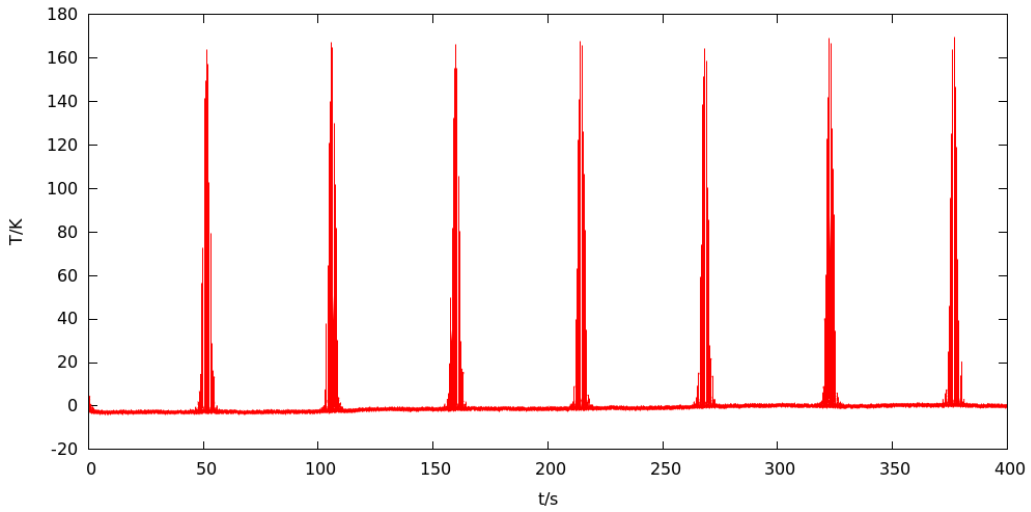

Figure 3: Data from a scan pattern of Jupiter converted to source brightness temperature. The peak heights are 165 K.

4 Noise Characterisation

Figure 4 gives the power spectrum of a channel of data produced by pointing the antenna at Mars. Being static, the data lacks the harmonics of a scan pattern, but is otherwise representative of all the data. It can be seen that there are two primary types of noise: atmospheric and electronic.

The constant, white noise component, is electronic in source. Thus, increasing the signal to noise ratio for this component will require increasing the data set. In addition, there is a peak at 50 Hz, which is the frequency of the Chilean mains. A filter can be applied to the data to remove this. The low frequency excess is due to atmospheric noise, with the zeroth order the largest. This is able to be removed by various methods, as discussed in section 5.

This accords with an examination of the Allen variance undertaken elsewhere.[6,7] This showed a slope at low Δt corresponding to white noise, a peak at large Δt due to atmospheric effects, and an excess between the two corresponding to the signal.

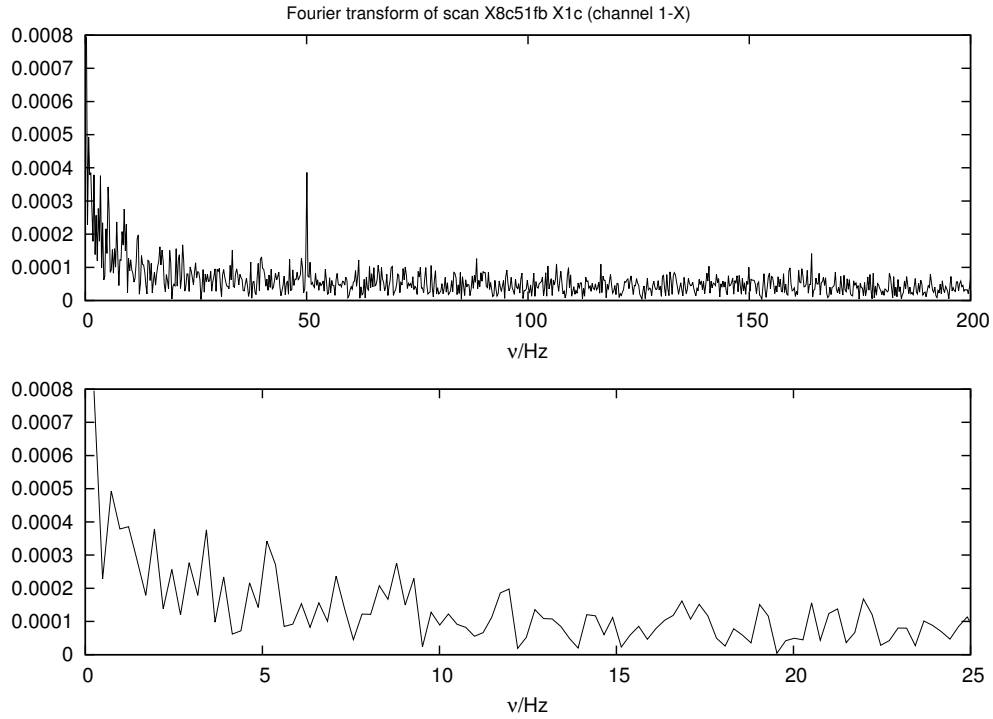

Figure 4: Fourier transform of a channel of data from Mars. The full frequency range is given on top, whilst an expanded view of the low frequency components is below.

5 Map Making and Noise Removal

5.1 Map Making

In principle, one can use observational data to directly produce constraints to astronomical parameters of interest. However, with large data sets, such as those here, this becomes computationally infeasible. Thus, the process of converting a long time-ordered dataset into a spatial temperature map of the sky can act as a useful data compression step.[5] Indeed, much of the work done on producing maps of CMB data is applicable here.[11,12]

The process of map making is that of transforming time-ordered into spatial data. Each pixel on the map receives a contribution from each data point with weight $w_{ij} = K(r_{ij})$, where r_{ij} is the distance from pixel i to data point j and K is the symmetric smoothing kernel, so equation 2 gives the total weight at a pixel. The kernel is a first order Bessel function multiplied by a Gaussian to limit ringing.

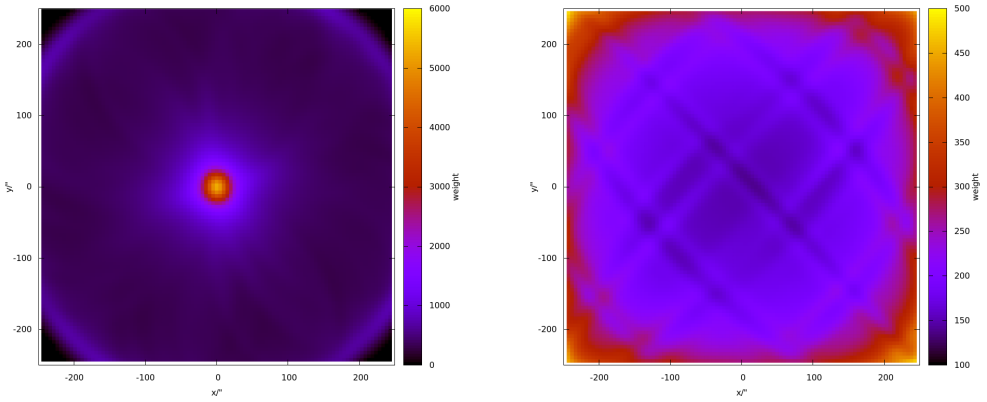

Figure 5: The weights of clover leaf (left) and Lissajous (right) patterns.

$$w_i = \sum_j K\left(r_{ij}\right) \tag{2}$$

The total weight is given in equation 2. This can be used to produce maps of the weight for the two scan patterns. As can be seen in figure 5, the smoothing kernel is needed to avoid gaps in the weight map. The Lissajous pattern produces an more even coverage, with a large weight at the edges, whilst the clover leaf pattern has a highly concentrated weight at the crossing point in the centre.

5.2 Noise Removal

5.2.1 Edge Methods

It is typically not a bad assumption that there should be no source signal at the edges of the map. Thus, one can split the data up into 'scans', with each scan starting at the edge of the map, and ending when it reaches the edge next. One can then add an offset and gradient to each scan to force both edges to be at zero.

Two methods were used, referred to as 'edge' and 'plane'. The edge method removed from each scan a gradient and an offset in time. The plane method removed the spatial plane that set both edges to zero and was nearest to the

horizontal. As figure 6 shows, both methods reduced the standard deviation of the noise, and ran in negligible additional time.

5.2.2 Basket Weaving

Basket-weaving is a technique to reduce striping image artefacts by offsetting scan lines to minimise the temperature differences at crossing points. Winkel, Flöer and Kraus developed an efficient algorithm to solve the basket weaving problem in the case where the number of data points is much larger than the number of pixels in the map.[9]

The scans are divided into two coverages of sizes I and J. Ideally, the number of crossing points between the two should be maximised. In this instance, the division was made according to the sign of the gradient of the scan.

Thus, one can calculate the vector of differences, $D_r = R_r\left[y^{(1)}\right] + R_r\left[y^{(2)}\right]$, where r is an index running over the $M \times N$ pixels in the map and $R\left[y^{(i)}\right]$ is the ith coverage mapped onto the sky. Then, neglecting noise and assuming that each coverage is the sum of the true sky temperature and an offset term for each scan ($p_j^{(i)}$), $D_r = R_r\left[p^{(1)}\right] + R_r\left[p^{(2)}\right]$.

Equation 3 gives the linear equation to be solved with a least squares method, where $w_r^{(i)}$is the total weight of the ith coverage at the rth pixel and $w_r\left(a^{(i)}\right)$ is the weight from the $a^{(i)}$th scan. This can be written as $\mathbf{D} = A\mathbf{P}$, where A is an $(M \times N) \times (I + J)$ matrix.

$$D_r = \frac{1}{w_r^{(1)}} \sum_{a^{(1)}} p_{a^{(1)}}^{(1)} w_r\left(a^{(1)}\right) + \frac{1}{w_r^{(2)}} \sum_{a^{(2)}} p_{a^{(2)}}^{(2)} w_r\left(a^{(2)}\right) \tag{3}$$

However, there is degeneracy in the solution for $\mathbf{P}$: one could add a constant offset, for example. Thus, one can solve for $\mathbf{P}$ by minimising the regularised expression $|A\mathbf{P} - \mathbf{D}|^2 + \lambda^2|\mathbf{P}|^2$, which can be done using a simple linear least squares algorithm.[3] The correction map is then given by equation 4.

$$C_r = \frac{\sum_{s=1}^{I} w_r^{(1)} A_{r,s} P_s + \sum_{s=I+1}^{I+J} w_r^{(2)} |A_{r,s}| P_s}{w_r^{(1)} + w_r^{(2)}} \tag{4}$$

λ is the dampening parameter. Figure 7 shows that there exists a wide range of values that leads to a consistent value for the standard deviation, with the lowest value near $\lambda = 0.1$, which was therefore chosen.

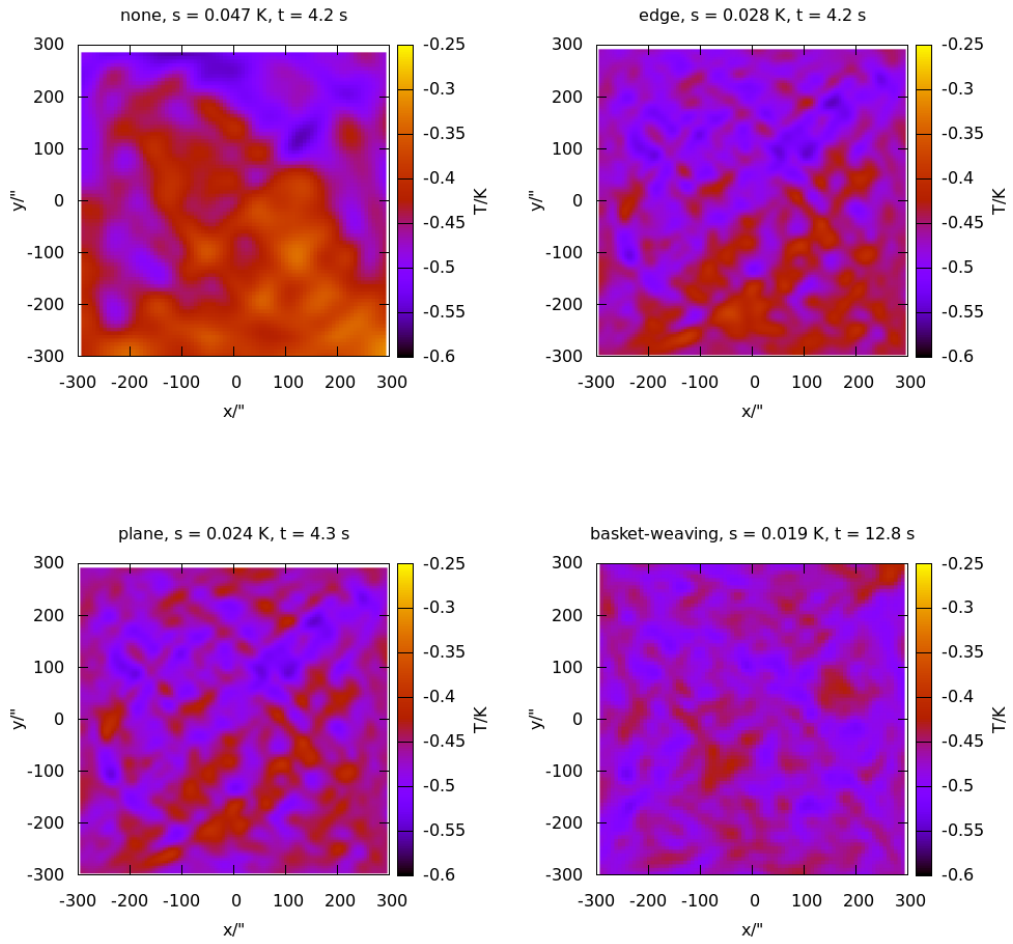

Figure 6: A comparison of three noise removal methods, with standard deviation and computational time given.

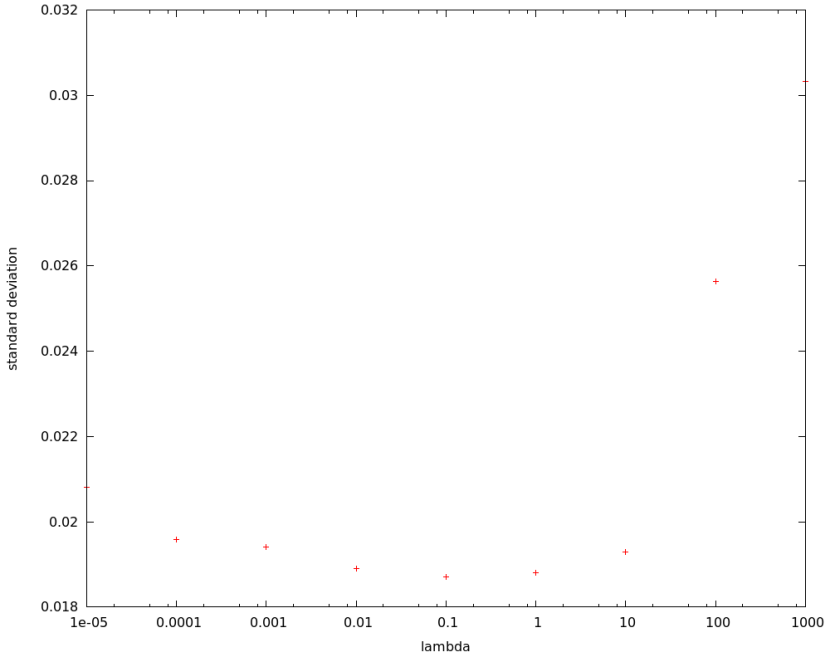

Figure 7: Effect of dampening parameter λ on the standard deviation of the basket woven output of an observation of blank sky.

The basket weaving method can be extended to treat arbitrary polynomial offsets by setting equation 5 as the new equation for D_r, where o_p is the maximum polynomial order, u_r (v_r) the data point number per scan line for coverage 1 (2), $1 \leq u_r \leq U_r$ ($1 \leq v_r \leq V_r$).

$$D_r = \sum_{o=0}^{o_p^{(1)}} p_{o,r}^{(1)} \left(\frac{u_r}{U_r}\right)^o + \sum_{o=0}^{o_p^{(2)}} p_{o,r}^{(2)} \left(\frac{v_r}{V_r}\right)^o \tag{5}$$

Then the same process as for $o_p = 1$ can be followed, producing the familiar matrix equation, but with A and $\mathbf{P}$ increased in size $(o_p + 1)$-fold. However, as can be seen in figure 8, a first order polynomial offset produces an inferior reduction in noise compared with a zeroth order offset, whilst increasing the computational requirements. Additionally, using a higher order polynomial will start to remove signal. Thus, $o_p = 1$ was used.

The method was tested using two images of the Orion Molecular Cloud (OMC) taken several months apart. As can be seen in figure 9, whilst they have the same form, the Lissajous pattern has its peak at a lower temperature. However, this is not unsurprising – the circular pattern has a higher

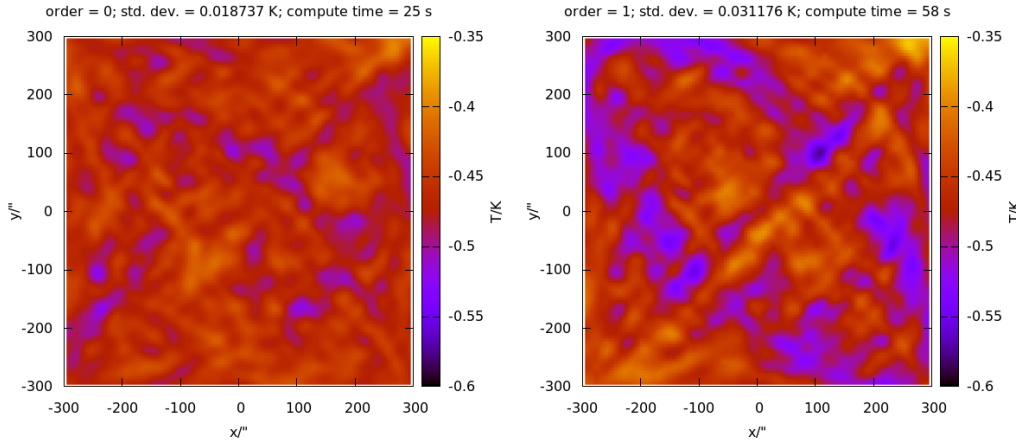

Figure 8: Effect of increasing polynomial order on the standard deviation and computational time for the basket woven output of an observation of blank sky.

weight at the centre, so will have a higher signal to noise ratio there. In addition, the Lissajous observation was taken with an antenna that was not tracking very well.

5.3 Discussion

5.3.1 Efficacy

As can be seen in figure 6, basket weaving produces the largest amount of noise reduction, lowering the standard deviation by 60%. The computational time is longer than for the other methods, but at 12.8s, would be very fast on good modern hardware.[1]

[1] All computation for this project was done using a computer with a 1.5 GHz Intel Celeron CPU running Ubuntu 14.10

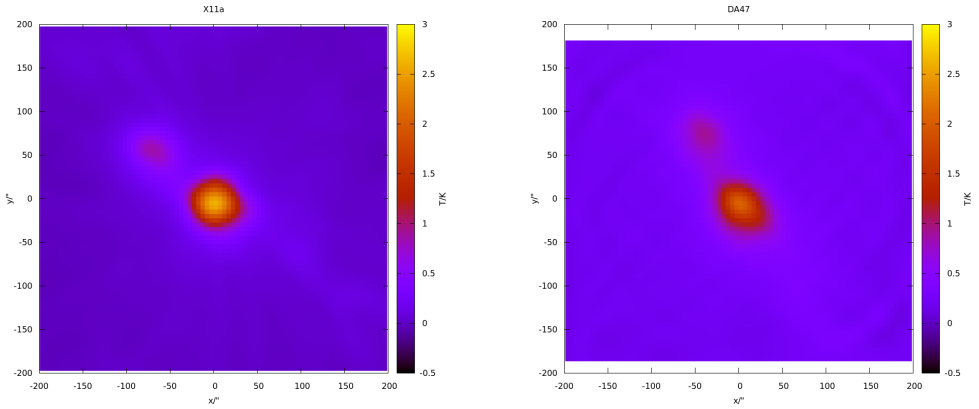

Figure 9: Two images of the Orion Molecular Cloud (OMC), both basket woven with the same parameters. X11a is a clover leaf pattern, whilst DA47 is a Lissajous pattern.

5.3.2 Future Work

There is certainly room for optimisation of the algorithms used. For example, the matrix A is approximately 90% sparse. Using a package designed for sparse matrices could reduce the memory and processor requirements.

5.3.3 Inference methods

Ideally, the map-making process should minimise the loss of information. It has been proved that inference methods can be chosen to lose no information.[5] One such is the method of Janssen & Gulkis,[11] which can be adapted for fast-scanning. Equation 6 gives a model for the measured temperature, T_m, at time t_i. $T_t(x_j)$ is the true sky temperature, whilst $A_{i,j}$ is the mapping between the two if there were no noise. Inference requires a model of the noise as Q functions of time, $f_q(t_i)$, with free parameters E_q, and N_i is random noise.

$$T_m(t_i) = \sum_j T_t(x_j) A_{i,j} + \sum_q E_q f_q(t_i) + N_i \tag{6}$$

This can then be written in the form of a matrix equation to be solved by

regularised least squares minimisation as in section 5.2.2. However, in this case, the matrix A will be of size $N_{\text{data}} \times (N_{\text{pixels}} + Q)$, which is 10^2–10^3 times larger than the matrix A used in basket weaving. Thus, this method will be substantially more computationally expensive. In addition, one would need a model for the atmospheric noise. However, inference is the most obvious next step in atmospheric noise removal from basket weaving, so merits further investigation.

6 Conclusions

Data from fast-scanning observations of multiple sources by ALMA have been analysed. The data was successfully converted into a brightness temperature format. The noise was analysed in the fourier domain, revealing a substantial atmospheric component.

Three methods of removing the atmospheric noise were investigated. Of these, basket weaving produced the most noise reduction (60%), whilst remaining computationally inexpensive.

There is scope for further work, refining the current basket weaving technique. In addition, inference may be a superior solution if computational speed is not a priority.

Acknowledgements

The author wishes to thank project supervisor Prof Richard Hills for many helpful discussions and also the ALMA project for providing the data.

References

[1] R E Hills & A J Beasely, *Proc SPIE*, 2008, **7012**, 70120N.

[2] T Kamazaki, S K Okumura, Y Chikada, T Okuda, Y Kurono, S Iguchi, S Mitsuishi, Y Murakami, N Nishimuta, H Mita & R Sano, *Publ Astron Soc Jpn*, 2012, **64**, 29.

[3] E Anderson, Z Bai, C Bischof, S Blackford, J Demmel, J Dongarra, J

Du Croz, A Greenbaum, S Hammarling, A McKenney & D Sorensen, *LAPACK Users' Guide*, 1999.

[4] A Wootten & A R Thompson, *Proc IEEE*, 2009, **97**(8), 1463–1471.

[5] M Tegmark, *ApJ Lett*, 1997, **480**, L87–L90.

[6] R E Hills, private communication.

[7] D W Allan, *IEEE Trans Instrum Meas*, 1987, **IM-36**(2), 646.

[8] A B Goldin, M S Kowitt, E S Cheng, D A Cottingham, D J Fixsen, C A Inman, S S Meyer, J L Puchalla, J E Ruhl and R F Silverberg, *ApJ Lett*, 1997, **488**, L161–L164.

[9] B Winkel, L Flöer & A Kraus, *A&A*, 2012, **547**, A119.

[10] A Kovacs, *Proc SPIE*, 2008, **7020**, 5.

[11] M A Janssen & S Gulkis, *The Infrared and Submillimeter Sky after COBE*, ed. M Signore & C Dupraz, 1992, 391.

[12] R Stompor, A Balbi, J D Borrill, P G Ferreira, S Hanany, A H Jaffe, A T Lee, S Oh, B Rabii, P L Richards, G F Smoot, C D Winant, J-H P Wu, *Phys Rev D*, 2002, **65**(2), 022003.